Framework for regional seismic risk assessments of groups of tall buildings

by James Bantis(1), Pablo Heresi(2), Alan Poulos(1), and Eduardo Miranda(1)

1 John A. Blume Earthquake Engineering Center, Department of Civil and Environmental Engineering, Stanford University, Stanford, CA, 94305, USA

2 Department of Civil Engineering, University of Chile, Santiago, Chile

***** Corresponding author
Email address: bantis@stanford.edu (J. Bantis)

Abstract

A novel probabilistic Monte Carlo-based framework to conduct regional seismic risk assessments using simplified continuous models is proposed. The hazard at rock outcrop is defined by response spectral ordinates which are simulated to account for spatial correlation and correlation across different periods simultaneously. For sites on firm and soft soils, a simplified site response analysis using a one-dimensional continuous nonuniform shear beam model is used to transform the hazard at rock outcrops to the hazard at all sites of interest. Uncertainty in the soil properties at each site is explicitly considered. Response spectra at each site are computed at the principal orientations of each building using recently proposed directionality models that permit the estimation of the seismic hazard at specific orientations. A one-dimensional continuous coupled shear-flexural beam model is used to simulate building dynamic properties accounting for modeling uncertainty and to obtain building responses for each building. The parameters of each model only require information on the building height and the lateral resisting system. All relevant uncertainties associated with each module of the framework are explicitly incorporated and propagated. Finally, a case study of tall buildings in San Francisco subjected to a magnitude 7.0 earthquake on the Hayward Fault is presented to illustrate how the framework can be implemented.

Keywords: Regional seismic risk assessment; reduced-order models; Monte Carlo simulation; continuous models; spatial correlation; ground motion directionality; modeling uncertainty.

1. Introduction

For almost 100 years, there has been an interest in regional seismic risk assessments. Freeman[1] performed one of the first studies into seismic loss estimation. Steinbrugge[2] summarizes some of the earliest earthquake loss estimation studies performed mainly by insurance companies. Reitherman[3] followed this by reviewing earthquake damage estimation methods in studies until the mid-1980s. For a review of seismic risk assessments and loss estimation methods before 2010, the reader is referred to Kircher et al.,[4] Aslani and Miranda,[5] Kircher et al.,[6] Calvi et al.,[7] and Scawthorn.[8] For a review of more recent seismic risk assessments, software, and methodologies, the reader is referred to Kassem et al.,[9] Hosseinpour et al.,[10] and Du et al.[11]

In recent years, much progress has been made in evaluating seismic performance. In particular, rational performance-based assessment methodologies have been developed, such as the Pacific Earthquake Engineering Research (PEER) Center's Performance-Based Earthquake Engineering (PBEE) framework. However, this methodology has been aimed at individual structures[12-14] and that is why it has also been referred to as a structure-specific seismic risk estimation methodology.[5] Furthermore, the PEER PBEE framework makes extensive use of nonlinear response history analysis of detailed finite element structural models. However, using these detailed models to conduct a seismic risk assessment for a large group of structures is not feasible, not only because of the large computational effort involved but, more importantly, because of the amount of detailed information required to develop the models. Instead, previous approaches at the regional level have made use of vulnerability functions based on expert opinion,[15] or have made estimates based on the response of single-degree-of-freedom (SDOF) systems together with empirical or expert-opinion fragility functions at the structure level.[16] However, evaluating the seismic response of buildings only using SDOF models does not capture the influence of higher modes, nor can it account for lateral deformation demands in certain stories. Furthermore, building classification systems in these approaches often

lump into a single building and fragility category structures with a range of heights that often have very different vulnerabilities.[17]

Heresi and Miranda[18] recently described the challenges in applying the original PEER framework at a regional scale. They highlighted how earthquakes, particularly large-magnitude events, strike large geographical areas, and when they occur near urban regions, they can affect hundreds or thousands of structures, resulting in major disruptions to society. Thus, from a societal point of view, we should be interested in the seismic performance of the built environment across a region in addition to the impact on individuals. They proposed an extension of the PEER PBEE framework for its use in groups of structures spatially distributed over a region, referred to as the Regional Performance-Based Earthquake Engineering (RPBEE) framework. Based on the RPBEE framework, the same authors proposed a novel seismic design approach, entitled regional-risk-targeted seismic design, where the design spectrum is modified to comply with locally defined regional seismic risk targets.[19]

In regional seismic risk assessments, the hazard is typically described using either Ground Motion Models (GMM) or physics-based simulated ground motions. However, for softer soil sites with high impedance contrasts, GMMs and physics-based simulations fail to adequately capture the strong amplifications of response spectral ordinates at periods at or near the modal periods of vibration of the soil deposit, sometimes referred to as site resonances. Furthermore, GMMs typically only provide a scalar measure of intensity at the site, such as the median of all horizontal orientations (i.e., RotD50),[20] and therefore neglect the important variations in ground motion intensity from one orientation to another.[21] In the case of buildings, the vast majority of structural elements (e.g., beams, structural walls, and bracing elements) and nonstructural elements (e.g., façades, interior partitions, and doors) have the same orientation as the principal axes of the structure. Therefore, our particular interest is to determine the seismic demands and seismic response of buildings in the principal axes of the structure, which, for most structures, are perpendicular to each other (e.g., transverse and longitudinal directions of a building). Recently, Poulos and Miranda[22] showed that the probability that the RotD50 intensity measure will be exceeded in one of these two orthogonal principal directions of a structure ranged from approximately 92% for short-period structures to 98% for long-period structures. Therefore, explicitly considering ground motion directionality is crucial to avoid underestimating seismic demands, seismic response, damage, and losses in some orientations and overestimation in other orientations. Furthermore, in many regional assessment methods (e.g., HAZUS[16]), spectral ordinates at different sites are typically assumed to be independent. However, important spatial correlations exist, particularly within urban areas where the distances from site to site are shorter than 20 km leading to systematic underestimations of seismic risk.[23] Therefore, sampling spatially correlated response spectral ordinates is necessary. Although some studies have incorporated the spatial correlation of spectral ordinates in regional seismic risk assessments,[24] they have only used mean correlations and have neglected their significant variability from one earthquake to another. Heresi and Miranda[25] recently developed the first spatial correlation model that incorporates this inter-event variability, but it has only been used in a few studies by the same authors.

The objective of this manuscript is to present a novel regional seismic risk assessment framework that extends the RPBEE framework developed by Heresi and Miranda[18] by using reduced-order models consisting of simplified continuous beams to estimate site and building responses that also explicitly incorporate ground motion directionality and modeling uncertainty. A probabilistic Monte Carlo approach is adopted to simulate the hazard at each site, to simulate building responses for each building, and to simulate possible damages for each response and structure when subjected to a scenario earthquake. Uncertainties associated with each portion of the framework are explicitly accounted for and propagated. In the proposed framework, response spectra at rock are simulated considering ground motion directionality, spatial correlation of spectral ordinates, and correlation of spectral ordinates across different periods at different sites. Site effects at soft soil sites are incorporated by conducting simplified site response analysis using non-uniform shear beam models, while realizations of building responses are obtained using a continuous coupled non-uniform shear-flexural beam model in combination with modal response spectrum analysis. The proposed regional framework is applied to a case study of 180 tall buildings in the city of San Francisco, California, subjected to a hypothetical magnitude 7.0 earthquake on the Hayward Fault, to illustrate the types of results that may be obtained from this framework.

2. Methods

The proposed regional seismic risk assessment framework includes a unique and novel combination of capabilities. Figure 1 summarizes the proposed framework to assess the seismic risk of a set of spatially distributed

buildings. Given an earthquake scenario and building locations, the assessment starts by sampling spatially and across periods correlated 5%-damped response spectral ordinates for each building for a reference rock outcrop. The soil properties of each site, specifically the depth to bedrock, are then used in a simplified site response analysis to transform the rock spectra into the response spectra at the surface of the soil profiles. Up to this point, all response spectra correspond to the median intensity from all horizontal orientations at a site, that is, what is referred to as RotD50.[20] The RotD50 spectra are then used to sample response spectra at the two principal orientations of each building by using a probabilistic directionality model. The dynamic properties of each building, that is, their modal periods, modal damping ratios, and effective mode shapes are then sampled using probabilistic models that are a function of the general building characteristics (e.g., building height and type of structural system) or estimated using measurements from ambient vibration or previous seismic events in the case of instrumented buildings. For each building, spectral ordinates are computed for the modal periods and damping ratios in both principal orientations by interpolating the sampled 5%-damped spectra and then using damping modification factors to obtain spectral ordinates for modal damping ratios different than 5%. These spectral ordinates are then used to perform modal response spectrum analyses for both principal orientations of each building and obtain peak floor accelerations and inter-story drift ratios along the height of each building. Finally, these building responses can be used to estimate the damage of structural or non-structural components within each building using fragility functions. All these steps are described in more detail in subsequent subsections.

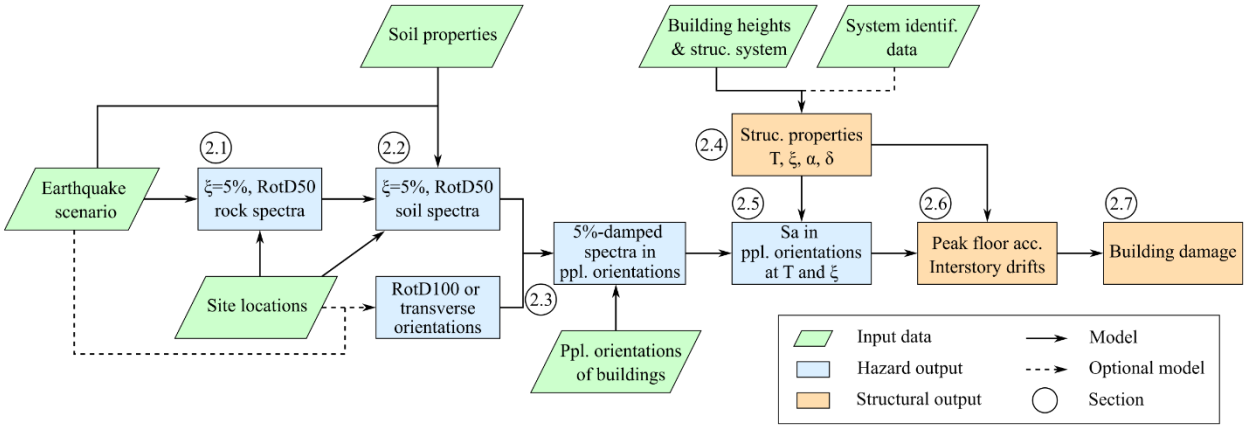

Figure 1: Methodological overview of the regional seismic risk assessment framework.

2.1 Ground motion modeling

Given that the largest source of uncertainty in regional seismic risk analyses typically resides in estimating ground motion intensity, it is particularly important how such intensity is estimated. In the proposed framework, this is done by sampling 5%-damped response spectral ordinates that are spatially correlated and correlated across periods at the location of each building for a given earthquake scenario. The response spectra are first sampled for a reference rock outcrop condition where it is first assumed that all sites have the same time-averaged shear-wave velocity to a depth of 30 meters, V_{s30}. These spectral ordinates correspond to the RotD50 values,[20] and are sampled using the following equation:

$$\ln \boldsymbol{Sa} = \boldsymbol{\mu}_{\ln Sa} + \boldsymbol{\varepsilon} \tag{1}$$

where $\boldsymbol{Sa}$ is a vector with pseudo-acceleration spectral ordinates at all periods and all sites, $\boldsymbol{\mu}_{\ln Sa}$ is a vector with the associated means of the logarithms of the pseudo-acceleration spectral ordinates estimated by using a ground motion model (GMM),[26] and $\boldsymbol{\varepsilon}$ is a multivariate normal random variable with zero mean and a covariance matrix that is constructed using the approximation proposed by Goda and Hong.[27] The covariance between spectral accelerations at two pairs of sites and periods, i and j, can be computed as:

$$cov(Sa_i, Sa_j) = \rho_0(T_i, T_j)\left[\tau(T_i)\tau(T_j) + \rho_w(\Delta_{ij}, \max\{T_i, T_j\})\sigma(T_i)\sigma(T_j)\right] \quad (2)$$

where T_i and T_j are the periods of interest at sites i and j, respectively; Δ_{ij} is the distance between both sites; τ and σ are the between-event and within-event standard deviation terms, respectively, which are also given by a GMM; ρ_0 is the correlation between spectral ordinates at two periods, for which several empirical models exist;[28] and $\rho_w(\Delta, T)$ is the within-event spatial correlation for the period T and distance Δ, which can be estimated using available models.[25,29-31] A more detailed description of the construction of the covariance matrix is given in the electronic supplement to this manuscript.

An important aspect to define at this stage is the set of periods at which the response spectra will be sampled. Enough periods are needed to have precise estimates of (i) the spectral moments used in the simplified site response analysis described in Section 2.2 and (ii) the interpolation required to obtain spectral ordinates at the modal periods of the buildings described in Section 2.5. However, using too many periods when sampling response spectra may increase the computational effort significantly due to the time involved in sampling multivariate normal distributions with a covariance matrix whose size is the product of the number of sites and the number of periods. A good compromise can be reached by sampling the response spectra at some of the periods used to fit the GMM and then interpolating the spectra at more periods to improve precision at the next steps. Based on a simple sensitivity analysis, 80 periods evenly spaced in logarithmic space from 0.01 to 10 s were enough to accurately conduct the site response analysis procedure presented in the next section.

2.2 Site response analysis

The 5%-damped RotD50 response spectra at reference rock outcrops are then used to obtain 5%-damped RotD50 response spectra at soil sites using a simplified site response analysis procedure. The simplified site response analysis procedure significantly improves the estimation of response spectra when compared to GMMs or physics-based ground motion simulations, particularly at softer soil sites with large impedance ratios. This section explains how the procedure can be implemented at the regional level for many sites by using only limited information at each site.

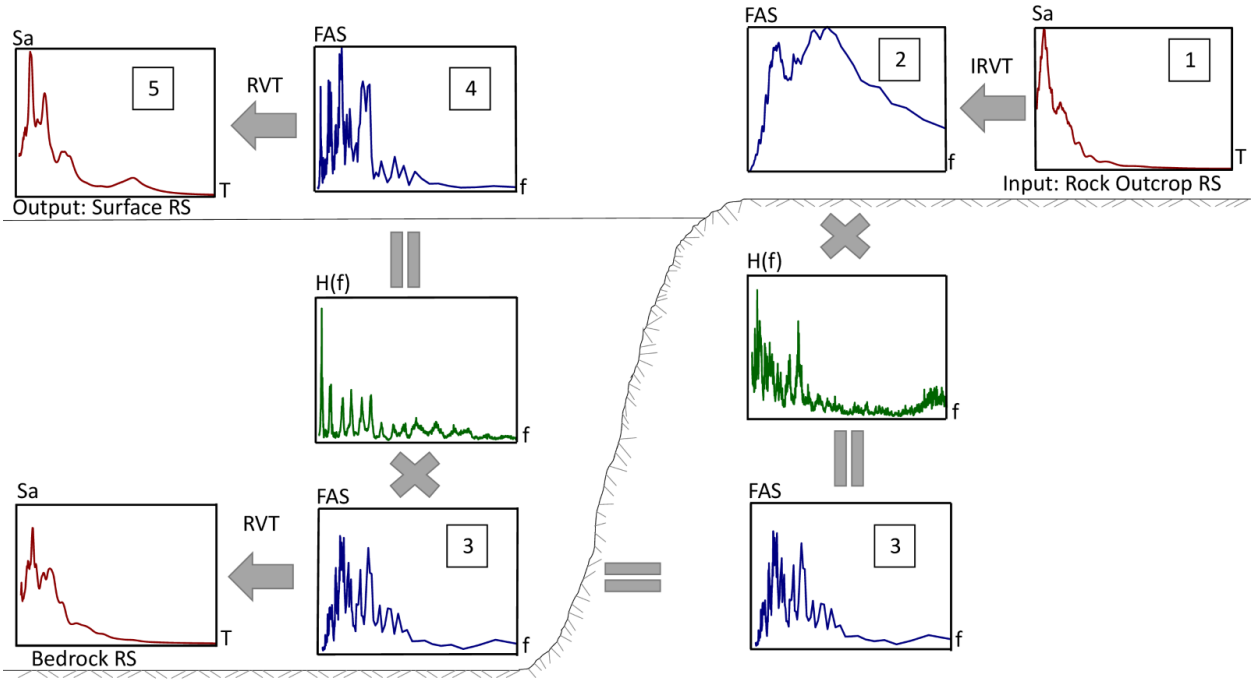

Figure 2: Simplified site response analysis used to transform a rock outcrop response spectrum into a response spectrum at the surface of a soil deposit.

Figure 2 outlines the simplified site response analysis procedure for transforming reference rock outcrop response spectra to ground surface response spectra at the sites of interest. The first step converts rock outcrop response spectra to Fourier Amplitude Spectra (FAS) through Inverse Random Vibration Theory (IRVT) based on the procedure first proposed by Gasparini and Vanmarcke.[32] For more information on conducting the IRVT, the reader is referred to the electronic supplement to this article and Rathje et al.[33]

After applying the IRVT procedure to the response spectrum at rock, multi-degree-of-freedom (MDOF) linear elastic transfer functions are used to first convert the FAS at rock surface to the FAS at bedrock through deconvolution and then convert the FAS at bedrock to the FAS at the ground surface through convolution. In this study, the term "rock model" describes the deconvolution, whereas the term "soil model" describes the convolution. It should be noted that in many past studies,[33] it is assumed that the rock outcrop FAS is the same as the bedrock FAS, but this is equivalent to assuming that the rock is rigid. Hence, this assumption tends to overestimate the ground motion intensity at soil sites because, given the flexibility of the rock, the motion at bedrock is somewhat less intense than that at the rock outcrop. The transfer functions to transform from rock outcrop FAS to bedrock FAS, $H(f)_{\frac{Bedrock}{Rock\ Outcrop}}$, and then bedrock FAS to ground surface FAS, $H(f)_{\frac{Soil\ Surface}{Bedrock}}$, are given by:

$$H(f)_{\frac{Bedrock}{Rock\ Outcrop}} = \sum_{j=1}^{n} \frac{\left(f_{Rock,j}^2 - f^2\right) + i\left(2\zeta_{Rock,j} f_{Rock,j} f\right)}{\Gamma\Phi_{Rock,j} f^2} \tag{3}$$

$$H(f)_{\frac{Soil\ Surface}{Bedrock}} = \sum_{j=1}^{n} \frac{\Gamma\Phi_{Soil,j} f^2}{\left(f_{Soil,j}^2 - f^2\right) + i\left(2\zeta_{Soil,j} f_{Soil,j} f\right)} \tag{4}$$

where the summation is performed over the n modes considered in the modal analysis, f is the frequency vector, $f_{Rock,j}$ is the j^{th} modal frequency for the rock model, $\zeta_{Rock,j}$ is the j^{th} modal damping ratio for the rock model, $\Gamma\Phi_{Rock,j}$ is the j^{th} effective mode at the top of the "rock" column, $f_{soil,j}$ is the j^{th} modal frequency of the soil model, $\zeta_{soil,j}$ is the j^{th} modal damping ratio of the soil model, and $\Gamma\Phi_{Soil,j}$ is the j^{th} effective mode at the surface of the "soil" column.

A simplified one-dimensional continuous shear beam model with a uniform distribution of mass and parabolic distribution of shear stiffness[34] is used to obtain the effective modes shapes $\Gamma\Phi_j$ and modal frequency ratios f_j/f_1 for both the "rock" and "soil" columns needed to obtain the two transfer functions shown in Figure 2. Figure 3a shows the Alonso-Rodriguez and Miranda[35] continuous model where a nonuniform pure shear beam is laterally coupled to a nonuniform flexural beam such that both beams undergo the same lateral displacement along the height. Figures 3b and 3c show the distribution of shear and flexural stiffness, respectively, along the normalized height with respect to the total height of the beam, x. As shown in this figure, the non-uniform shear beam is assumed to have a parabolic distribution of stiffness, while the flexural beam has a distribution given by a quadratic function. These distributions were selected by Alonso-Rodriguez and Miranda[35] to allow a closed-form solution to the dynamic parameters of the coupled non-uniform shear-flexural model. The nondimensional parameter, α, controls the degree of participation of overall flexural and shear deformations in the model, and it is computed as the ratio between the shear and flexural stiffnesses at the base of the model ($\frac{GA_0}{EI_0}$). To model the "soil" and "rock" columns, only the shear beam portion of Figure 3a is considered. Therefore, α can be taken as infinity for the simplified site response analysis. The continuous model of Figure 3a is again used in Sections 2.4 and 2.6 to model building responses using different values of α. The variation of the lateral stiffness along the shear beam shown in Figure 3b is controlled only by the nondimensional parameter δ, which is the ratio between the shear stiffness at the top of the beam and the one at the bottom of the beam. The modal frequency (or period) ratios and effective modal shapes at any normalized depth with respect to the depth to bedrock (D_b) can be obtained in closed form or numerically only as a function of δ. Note that the height of the beam (H) in Figure 3 is equal to the depth to bedrock (D_b) for the site response analysis procedure. Therefore, to obtain the two transfer functions given by Equations (3) and (4), a small set of variables is needed: the nondimensional parameter δ, the predominant period of the site (T_g), the depth to bedrock (D_b), and the modal damping ratios of both the "soil" and "rock" columns. As an alternative to the predominant period of the site, one can use the "equivalent homogeneous shear wave velocity" model instead.[36] Ideally, these parameters are obtained deterministically by system identification using records from downhole arrays for specific sites of interest. For the regional problem at hand, where most sites may not have downhole array data, the unknown parameters are determined using the sites in the region with available data.

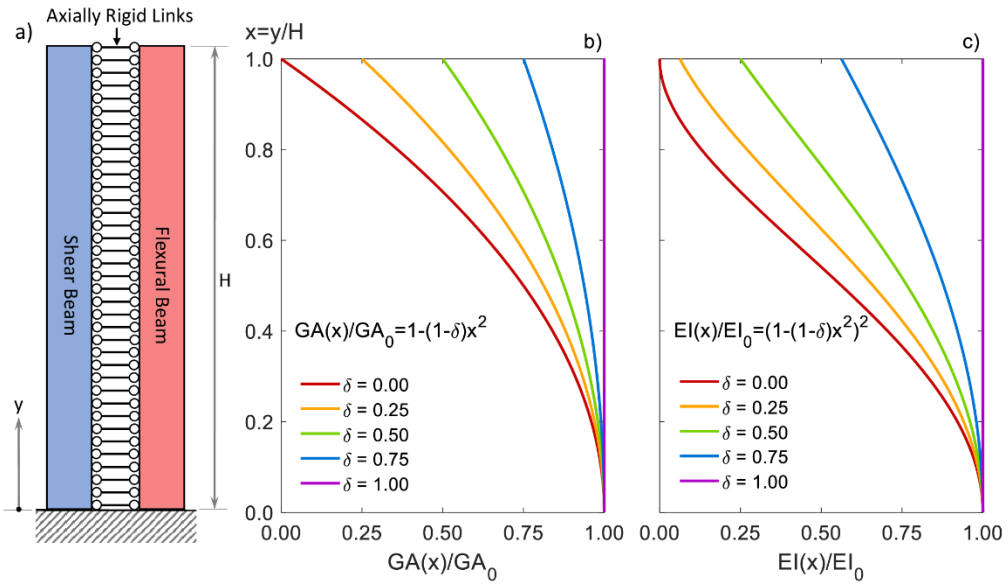

Figure 3: (a) Continuous coupled flexural and shear beam model; distribution of (b) shear and (c) flexural lateral stiffness along the height of the model as a function of δ.

When the predominant period of the site is unknown, it can be obtained from the equation of the first (fundamental) period of vibration of a uniform shear beam model of uniform damped soil on rigid rock given by:

$$T_g = \frac{4D_b}{V_s^*} \tag{5}$$

where D_b is the depth to bedrock at the site of interest and $V_s^\star$ is the equivalent homogeneous (uniform) shear wave velocity. Herein, V_s^* was obtained by solving Equation (5) for instrumented sites where the depth to bedrock, D_b, is known and T_g is determined from system identification techniques. The equivalent homogeneous shear wave velocity, V_s^*, was then used to obtain samples of T_g at non-instrumented sites where the depth to bedrock is known, explicitly considering uncertainties in V_s^* and D_b. The parameter δ was taken as deterministic, with its value set as the geometric mean δ of instrumented sites in the region of interest. Note that the non-uniform shear beam model used here differs from the one with a generalized parabolic model for the variation of shear wave velocity whose solution is in terms of Bessel functions.[37] In the non-uniform model used herein, the parabolic variation is on the lateral shear stiffness, and the solution is in terms of associated Legendre functions. Modal damping ratios were sampled from a lognormal distribution where the median and dispersion parameters for each mode were estimated from the sites with downhole array records. The electronic supplement of this article provides more detailed information on the sampling of the soil and rock model parameters.

The final step in the simplified site response analysis procedure is shown in the upper left corner of Figure 2 and involves using Random Vibration Theory (RVT) to transform the FAS at the surface of the soil deposit of interest to the response spectrum. The specific RVT procedure is based on results from Bantis and Miranda[38] aimed at estimating response spectra at soft soil sites and is described both in the electronic supplement of this article and in Bantis and Miranda.[38]

Figure 4 shows an example of the effect of depth to bedrock on the seismic hazard at three hypothetical sites. Figure 4a provides the 5%-damped pseudo-acceleration response spectrum for the RotD50 orientation of the motion recorded during the 1989 Loma Prieta earthquake at the Rincon Hill station. This station was located at a rock outcrop in the southeastern corner of the Financial District of the city of San Francisco and its response spectrum is used as the input to the simplified site response analysis procedure. The transfer functions modeling the rock and soil columns were computed using five modes and calibrated parameters for the San Francisco area (to be discussed in the case study). Figure 4b shows the soil model transfer functions for three sites with different depths to bedrock. As expected, the site with a larger depth to bedrock has a larger predominant period of the soil deposit, based on Equation (5). The 5%-damped pseudo-acceleration response spectra computed for the surface of soil deposits for these three hypothetical sites are shown in Figure 4c, showing that a greater depth to bedrock leads to a greater T_g of the soil deposit and more amplified spectral ordinates at longer periods.

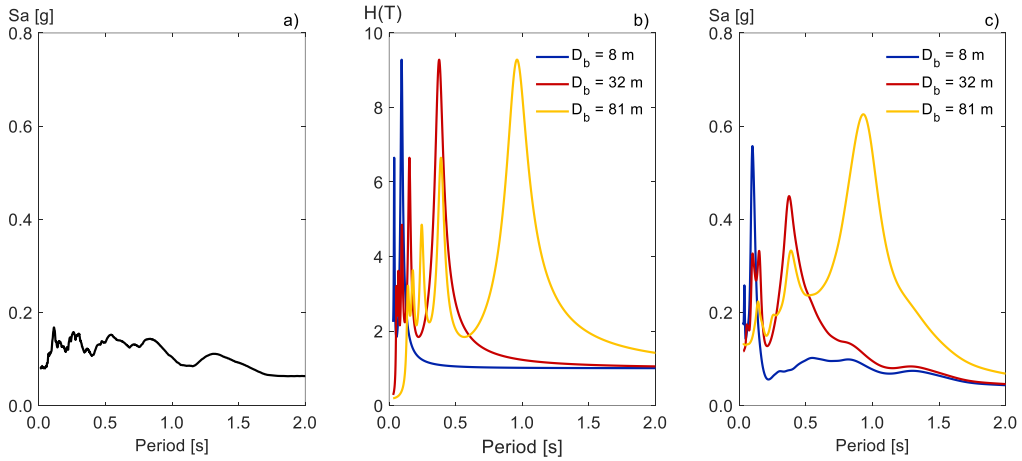

Figure 4: Effect of the depth to bedrock on the overall site response analysis procedure: (a) input 5%-damped pseudo-acceleration response spectrum for the RotD50 orientation of the Loma Prieta earthquake at Rincon Hill; (b) soil model transfer functions, $H(T)_{\frac{Soil\ Surface}{Bedrock}}$, for three sites with different depths to bedrock; (c) output 5%-damped pseudo-acceleration response spectra at the three sites.

2.3 Ground motion directionality

Up to this point, all response spectra discussed so far at rock and soil sites correspond to the median from all horizontal orientations (i.e., RotD50). However, due to their geometry and arrangement of lateral load-resisting elements, buildings usually have two principal orientations, denoted here as P_1 and P_2, which are typically orthogonal to each other. Response spectral ordinates in specific orientations, such as the principal orientations of buildings, can be significantly higher or lower than RotD50 spectral ordinates. In the proposed regional seismic risk assessment, one of two alternate methods is used to explicitly account for ground motion directionality, transforming RotD50 response spectral ordinates into response spectral ordinates in the P_1 and P_2 orientations of each building. These methods are shown schematically in Figure 5. The first method starts by defining the orientation of maximum intensity (RotD100). Some alternatives that can be used to define this orientation are to sample it from a uniform distribution or by using the empirical distribution defined by Shahi and Baker[39] for sites with rupture distances shorter than 5 km, estimate it using recorded ground motions, or fix it to a user-defined value. Angular distances between the orientation of RotD100 and both principal orientations of each building are then computed, denoted herein as ϕ_1 and ϕ_2 in Figure 5a. Finally, spectral ordinates at each principal orientation are obtained by multiplying the RotD50 spectral ordinates by ratios empirically derived by Poulos and Miranda[21] and given by:

$$Sa(T,\phi) = Sa_{RotD50}(T)\nu(T,\phi) \quad (6)$$

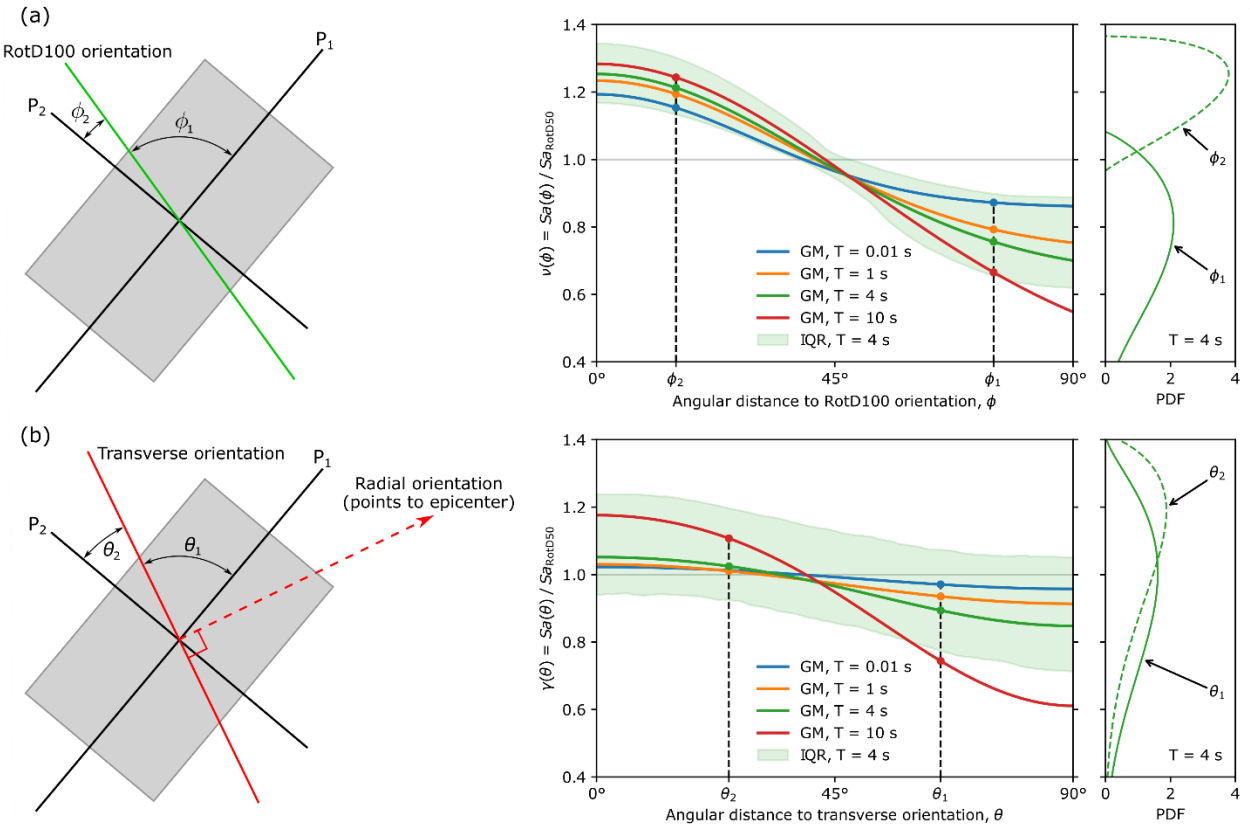

Figure 5: Sampling scheme used to explicitly account for ground motion directionality to obtain response spectral ordinates at the orientations corresponding to the principal axes of a building (P_1 and P_2) when knowing: (a) the orientation of RotD100 and (b) the transverse orientation.

where $Sa(T,\phi)$ is a sampled spectral ordinate at period T in an orientation that is at an angle ϕ away from the RotD100 orientation, Sa_{RotD50} is the RotD50 spectral ordinate, and $\nu(T,\phi)$ is a modification factor to account for ground motion directionality which is sampled from a four-parameter Beta distribution with parameters that were calibrated by Poulos and Miranda[21] using shallow crustal earthquakes in active tectonic regimes. Figure 5a shows the geometric mean of ν for four different periods and all possible orientations as well as the probability density function for ν for a 4s period for the two angles ϕ_1 and ϕ_2.

The second method that can be used to sample response spectral ordinates in the P_1 and P_2 orientations stems from the fact that, for strike-slip earthquakes, the orientation of the maximum response spectral ordinate (i.e., RotD100) tends to occur close to the transverse orientation, especially at long periods.[40] Thus, the first step is to compute the transverse orientation at the location of each building, which is perpendicular to the orientation that points towards the earthquake epicenter. Angular distances between the transverse orientation and both principal orientations of each building are then computed, denoted herein as θ_1 and θ_2 in Figure 5b. Finally, spectral ordinates at each principal orientation are then sampled similarly to the previous method by using the following equation:

$$Sa(T,\theta) = Sa_{RotD50}(T) \cdot \gamma(T,\theta) \tag{7}$$

where $Sa(T,\theta)$ is a sampled response spectral ordinate at period T in an orientation that is θ away from the transverse orientation and $\gamma(T,\theta)$ is a modification factor to account for ground motion directionality which is sampled from a scaled Beta distribution whose parameters were calibrated by Poulos and Miranda[41] using empirical data. Figure 5b shows the geometric mean of γ for four different periods and all possible orientations as well as the probability density function for the modification factor γ for a 4s period for the two angles θ_1 and θ_2.

2.4 Probabilistic characterization of dynamic properties of buildings

In the proposed regional seismic risk assessment framework, buildings are modeled using a reduced-order model shown in Figure 3, consisting of a non-uniform shear-flexural beam model. The response is assumed to be uncoupled in perpendicular directions. In each direction, the model is fully defined by four parameters which must be sampled for each building to explicitly account for modeling uncertainty. These are: the fundamental period (T_1), 1st modal damping ratio (ζ_1), the lateral stiffness ratio α which mainly depends on the type of lateral resisting system in the building, and the parameter δ. There are three ways to obtain these parameters depending on the information available for each building. For buildings that are seismically instrumented and have recorded responses throughout their heights from previous earthquakes, system identification techniques may be used to obtain the four parameters that minimize the difference between computed and recorded responses. For all other buildings, α is sampled from a uniform distribution with parameters that depend on the building's structural system, whereas δ is taken as a deterministic function of building height. For buildings with limited information, where only the structural system and height are known, the fundamental periods and first modal damping ratios in each principal orientation are sampled simultaneously, accounting for the correlations between these variables in both principal orientations. The probability distributions used for sampling fundamental periods and first modal damping ratios as a function of building height and lateral resisting system were fitted using data from Cruz.[42] For buildings with recorded ambient vibrations, this information is used to reduce the uncertainty in estimating the fundamental period of the building. For these buildings, the fundamental periods and first modal damping ratios are sampled independently. The reader is referred to the electronic supplement for detailed information on how the four parameters in each principal orientation of each building are obtained for the three situations.

Once T_1, ζ_1, α, and δ are sampled for each building and direction, modal period ratios and effective mode shapes can be computed using the continuous coupled shear and flexural beam model of Figure 3. Alonso-Rodriguez and Miranda[35] derived analytical solutions for both these values. Alternatively, the continuous model can be discretized as an MDOF, and the modal period ratios and effective mode shapes can be computed by solving the eigenvalue problem numerically, which is the approach used herein. Higher modal periods are then obtained by multiplying the sampled fundamental period of vibration, T_1, by the computed modal period ratios.

To obtain samples of the modal damping ratios for the higher modes of vibration, the Cruz and Miranda[43] equation dependent on the first modal damping ratio and modal period ratios is used, which is given by:

$$\zeta_j = \zeta_1 \left(1 + \lambda \left(\frac{T_1}{T_j} - 1\right) + \epsilon\sigma_s\right) \tag{8}$$

where λ and the standard error, σ_s, are constants dependent on the structural system in the Cruz and Miranda[43] model, T_j is the sampled period of the j^{th} mode, ζ_j is the sampled modal damping ratio of the j^{th} mode, and ϵ is sampled from a truncated standard normal distribution between -2.5 and 2.5. For instrumented buildings with recorded responses from prior earthquakes, the higher modes can be obtained either directly using system identification techniques, or from Equation (8).

2.5 Spectral ordinates at modal periods and modal damping ratios

As described in Section 2.3, the 5%-damped response spectra in the principal orientations of each building were computed for a pre-established vector of periods of vibration common to all sites of interest. However, these periods do not necessarily correspond to the modal periods in each direction of the buildings. Thus, it is necessary to interpolate from those spectral ordinates to obtain the 5%-damped spectral ordinates at the sampled modal periods for each building and each of the two principal directions. The response spectral ordinates corresponding to the sampled modal damping ratios, $Sa(T, \zeta)$, are then computed by multiplying the 5%-damped response spectral ordinates, $Sa(T, \zeta = 5\%)$, by a damping modification factor (DMF), C_ζ, as follows:

$$Sa(T_j, \zeta_j) = C_\zeta \cdot Sa(T_j, \zeta = 5\%) \tag{9}$$

where $Sa(T_j, \zeta_j)$ is the spectral ordinate at a period of the j^{th} mode with a damping ratio equal to the modal damping ratio of the j^{th} mode and $Sa(T_j, \zeta = 5\%)$ is the spectral ordinate at a period of the j^{th} mode with a damping ratio of

5%. There are many different DMF models the analyst can use depending on the region of study.[44-47] Rezaeian et al.[44] and Rezaeian et al.[45] concluded that site conditions have a small effect on DMFs, however, in the case of structures built on soft soils, DMFs are significantly different and using the DMFs proposed by either Dávalos et al.[46] or Bantis and Miranda[47] is recommended.

An example of how to obtain the spectral ordinates at the modal periods and modal damping ratios of interest for the Millennium Tower in the Financial District of San Francisco is shown in Figure 6. For this structure, which is seismically instrumented, system identification techniques were adopted using recorded responses in various earthquakes to infer the first four modal periods and modal damping ratios in both principal directions of the building. Figure 6a shows the median DMFs proposed by Bantis and Miranda,[47] which were specifically developed for soft soil sites in the San Francisco Bay Area and are computed as a function of the damping ratio and the ratio between the period of vibration of interest and the predominant period of the soil deposit. The predominant period of the soil deposit for this site was identified using the simplified models proposed by Bantis and Miranda.[47] The median DMF ordinates for the first four modes in the Northwest-Southeast principal orientation of this building calculated using the DMF model proposed by Bantis and Miranda[47] are indicated as black points in Figure 6a. Figure 6b shows the 5%-damped pseudo-acceleration response spectrum of the 2014 M_w 6.0 South Napa earthquake at the base of the Millennium Tower in its Northwest-Southeast principal component. Red points indicate the first four modal response spectral ordinates obtained from multiplying the 5%-damped pseudo-acceleration response spectrum by the corresponding DMF ordinates in Figure 6a. Note that the second mode of vibration of the building practically coincides with the predominant period of the site, and therefore there is a strong amplification of that spectral ordinate as a result of a modal damping ratio smaller than 5%, whereas for the other three modes shown in this figure, the change in damping ratio does not introduce significant variations in seismic demands. Although median DMFs are used in the example shown in Figure 6, the proposed regional analysis uses realizations of DMFs sampled from lognormal distributions using dispersions provided in DMF models.[44,47]

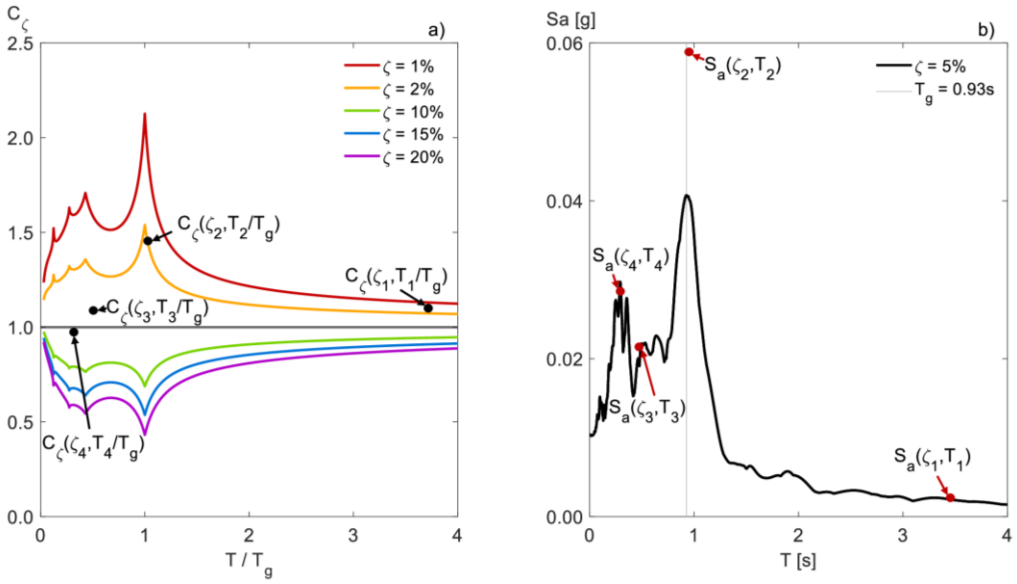

Figure 6: Effect of changes in the damping ratio on the first four modal response spectral ordinates for the Northwest-Southeast principal component of the Millennium Tower: (a) median DMFs proposed by Bantis and Miranda[47] indicating modification factors for the first four modes; (b) 5%-damped pseudo-acceleration response spectrum of the 2014 South Napa M_w 6.0 earthquake and modified spectral ordinates of the first four modes.

2.6 Structural response

To compute engineering demand parameters (EDPs) along the heights of each building and in each principal orientation, a modal response spectral analysis is adopted by using the response spectral ordinates at the periods and damping ratios corresponding to each realization of the building model. Story drift ratios (SDRs) and peak floor accelerations (PFAs), two of the most commonly used EDPs to assess damage in structural and nonstructural

components in buildings, are computed either at heights corresponding to stories/floors in each building or continuously from the base to the roof.

Because most tall buildings tend to be regular in plan to minimize the torsional response, they usually have well-separated modes. Furthermore, since the contribution of higher modes in response parameters dependent on story drifts tends to be strongly dominated by the first mode of translation in each direction, then the sum root sum square (SRSS) modal combination rule provides relatively good approximations and therefore SDRs can be computed as follows:[48]

$$SDR_k \approx \frac{1}{H}\sqrt{\sum_{j=1}^{n}\left(\Gamma\Phi'_{k,j}\, Sd_j\right)^2} \tag{10}$$

where SDR_k is the SDR of the k^{th} story, $\Gamma\Phi'_{k,j}$ is the derivative of the effective modal shape with respect to height at the k^{th} story for the j^{th} mode, Sd_j is the spectral displacement for an oscillator with a period of vibration and a damping ratio corresponding to those of the j^{th} mode, computed as described in Section 2.5, H is the building height, and n is the number of modes considered in the analysis. For most buildings, considering three modes in each direction is enough to estimate SDRs.

To compute PFAs, considering more modes is necessary, but for most buildings, six modes in each principal direction are enough. More importantly, even if modes are well separated, the SRSS modal combination should be used, since significant correlations may exist between modal responses of modes in the high-frequency region[49] and therefore, the complete quadratic combination (CQC) rule may underestimate the response. Moreover, even the extended CQC method may not correctly estimate peak absolute accelerations whose adequate estimation depends not only on the correlation of oscillator responses relative to the ground but also requires consideration of the correlation between peak ground accelerations and relative accelerations. As a result, the approach from Taghavi and Miranda,[50] which considers the correlation between modal relative accelerations as well as between relative accelerations and ground accelerations, is suggested instead. In the response spectrum method developed by Taghavi and Miranda,[50] the peak acceleration at the floor k, PFA_k, is estimated as follows:

$$PFA_k \approx \Big(\Big(1-\sum_{j=1}^{n}\Gamma\,\Phi_{k,j}\Big)^2 PGA^2 + \sum_{i=1}^{n}\sum_{j=1}^{n}\rho_{ij}\,\Gamma\,\Phi_{k,i}\,\Gamma\,\Phi_{k,j} Sa_i Sa_j + 2\Big(1-\sum_{j=1}^{n}\Gamma\,\Phi_{k,j}\Big)PGA\sum_{j=1}^{n}\rho_{jg}\Gamma\,\Phi_{k,j}Sa_j\Big)^{0.5} \tag{11}$$

where PGA is the peak ground acceleration, Sa_i and Sa_j are the pseudo-acceleration response spectral ordinates for the i^{th} and j^{th} modes, respectively, computed as described in Section 2.5, ρ_{ij} is the correlation between total accelerations of two modes of vibration i and j, and ρ_{jg} is the correlation between the ground acceleration and total modal acceleration of the j^{th} mode. Details of these correlation factors can be found in the electronic supplement.

2.7 Building damage

The probability of damage to structural and non-structural components of the buildings, as well as to different contents within the building, is calculated by using fragility functions and the individual realizations of PFAs and SDRs along the height of a building computed as described in the previous section. The results are given in terms of the probability that a given component type will have a particular damage state or higher. Some example fragility functions that can be used for this purpose are those developed by Ramirez et al.[51] for pre-Northridge welded steel moment-resisting beam-to-column connections, Miranda and Mosqueda[52] for cold-formed steel framed gypsum wall-board partition walls, and many others available in the FEMA P-58 background documentation.[53] Note that, at a regional scale, seismic damage can also be spatially correlated.[54] However, as damage is estimated at the component level in the proposed framework, no structure-to-structure damage correlation was considered in this article.

3. Case study illustrating the use of the framework

To illustrate the use and type of results of the proposed regional seismic risk assessment framework, it was applied to a portfolio of 180 tall buildings located in the Financial District of the city of San Francisco, California. The heights

of these buildings are all greater than 45 m, with 156 buildings having heights greater than 73 m. Building heights and lateral resisting systems were obtained from the San Francisco Tall Buildings Study.[55] The buildings were subjected to the HayWired scenario,[56] which consists of a hypothetical M_w 7.0 strike-slip earthquake on the Hayward Fault with an epicenter at (37.800°, 122.180°).

The Boore et al.[26] GMM was used to sample 5%-damped response spectra for all 180 sites by first considering all the sites as reference rock outcrops with V_{s30} = 760 m/s, which is a typical value used for reference rock sites.[57] The Afshari and Stewart[58] ground motion duration model was used to estimate the significant durations required for the simplified site response analysis. The equivalent homogeneous shear wave velocity, $V_s^\star$, was taken to be 338 m/s, which was obtained by using the depth to bedrock and the predominant period of the site, T_g, at ten instrumented sites with available records in the Financial District of San Francisco. Models to sample the δ parameter and the modal damping ratios for the soil and rock columns were fitted using records from five sites with downhole arrays in the San Francisco Bay Area. Further details of these models are presented in the electronic supplement of this article. Six modes were considered in the transfer functions and modal analyses discussed in Section 2.2 and given by Equations (3) and (4).

To modify the RotD50 spectra at each site to realizations of response spectra in the orientation of the principal components of each building, individual realizations of the modification factor $\gamma(T,\theta)$, which has a four-parameter Beta distribution, was used in combination with Equation (7). This modification factor depends on the angular difference between the orientation in each principal direction of each building and the transverse orientation. Since the HayWired scenario is a strike-slip event, the orientation of maximum spectral response is expected to occur close to the transverse orientation.[40]

Individual realizations of building response in each principal direction of each building were computed using response spectrum analysis considering the first six translational modes. Building properties were sampled using system identification for eleven instrumented buildings whose properties were treated as deterministic. Ambient vibration data on ten buildings from Byerly et al.[59] were used to reduce the uncertainty in modal building periods, and the dynamic properties of the remaining 159 buildings were sampled using the limited information approach where modal periods, modal damping ratios, and effective mode shapes are obtained from probabilistic models based on the building height and lateral resisting system. The Bantis and Miranda[47] DMFs were used for sites with V_{s30} values less than or equal to 220 m/s, whereas the Rezaeian et al.[44] DMFs were used for sites with V_{s30} values greater than 220 m/s.

Probabilities of damage in structural and nonstructural elements were simulated along building heights for each principal direction of each building. Herein, damage realizations are presented for yielding of beam-column connections for steel moment resisting frame (SMRF) buildings, minor cracking of gypsum partition walls, and significant cracking of gypsum partition walls. For this purpose, fragility curves were obtained from Ramirez et al.[51] for yielding of pre-Northridge beam-column connections in SMRF buildings and from Miranda and Mosqueda[52] for both minor and significant cracking of gypsum wall-board partition walls.

The effect of uncertainty on spectral ordinates and the large variations in frequency content across short distances are highlighted in Figure 7. Figure 7a shows 5%-damped RotD50 pseudo-acceleration response spectra for three sites, marked on the depth to bedrock contour map of downtown San Francisco obtained from Schlocker et al.[60] in Figure 7b. The medians and interquartile ranges of the response spectra from 1,000 simulations for each of the three sites are shown in Figure 7a. Figure 7b shows how the depth to bedrock can change rapidly in downtown San Francisco for sites within very short distances of one another. For example, the depth to bedrock changes by 73 m from Site A to Site C with a separation distance of approximately 580 m. The predominant period of the soil deposit is inversely proportional to the depth to bedrock (see Equation 5), and therefore, not only changes this value but produces significant changes in spectral ordinates across short distances, as demonstrated by Figure 7a. For example, on average, Site C, which is located close to the rock outcrop at Rincon Hill, has response spectral ordinates that are much lower than those at Site A at periods approximately between 0.15 s and 2.0s. Because the first few modal periods of high-rise buildings are usually longer than 0.15 s, the building responses and damages are expected to be much greater for a high-rise building at Site A than at Site C.

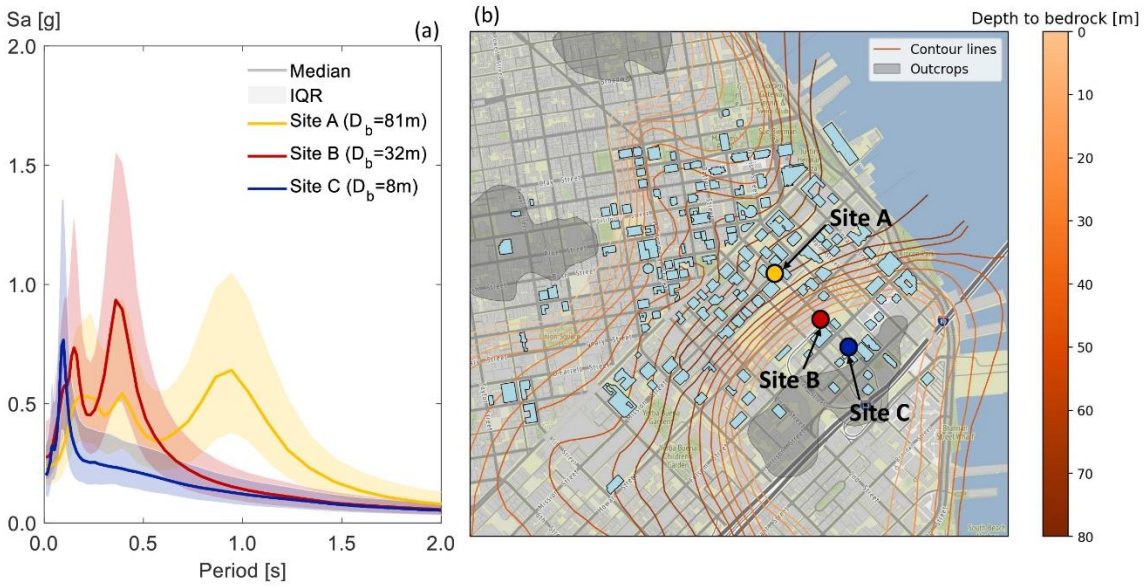

Figure 7: Effect of uncertainty on spectral ordinates and depth to bedrock on simulated response spectra: (a) simulated 5%-damped RotD50 pseudo-acceleration response spectra at three sites; (b) contour map of depth to bedrock in downtown San Francisco indicating the three sites.

Multiple realizations of building EDPs throughout the heights of all 180 buildings considered were simulated for each of their principal directions. Figures 8a and 8b show examples of SDR profiles for two buildings whose locations are indicated on the building height map of Figure 8c. The SDRs shown in these figures correspond to the maximum of the two principal directions of the buildings at each story. In addition to 100 individual realizations shown in thin light gray lines, the figure also indicates SDR profiles corresponding to the medians and interquartile ranges computed over 1,000 simulations. Please note that for clarity purposes individual realizations are shown for only 100 simulations and not the 1,000 that were used for computing the median and interquartile demands. Individual realizations provide information on the large variability that exists in seismic demands when the various modeling uncertainties are considered. Uncertainty sources include not only the estimation of ground motion intensity at the rock outcrop but also site and building response analyses. Building A has 43 stories and a height of 184 m while Building B has 13 stories and a height of 51 m. The effect of the number of stories (or building height) on the shape of the SDR profile is shown very clearly in Figure 8. For the shorter building (Building B), the SDR is primarily dominated by the first translational modes and the resulting median SDR profile along the height is relatively uniform, whereas the second mode, which has a large derivative with respect to height in the upper 20% of the building,[35] produces large SDR demands near the top for the taller building (Building A). This higher contribution of the second mode leads to a median SDR profile with deformation demands increasing from the base of the building to a peak near the top of the building and then decreasing again for the taller building. The strong contribution of the second mode in the upper portion of this building is the result of the modal period of the second mode occurring very close to the predominant period of the site. This occurs for Building A because it is tall enough and, as illustrated in Figure 7b, is situated on soil with a large depth to bedrock (approximately 80 m).

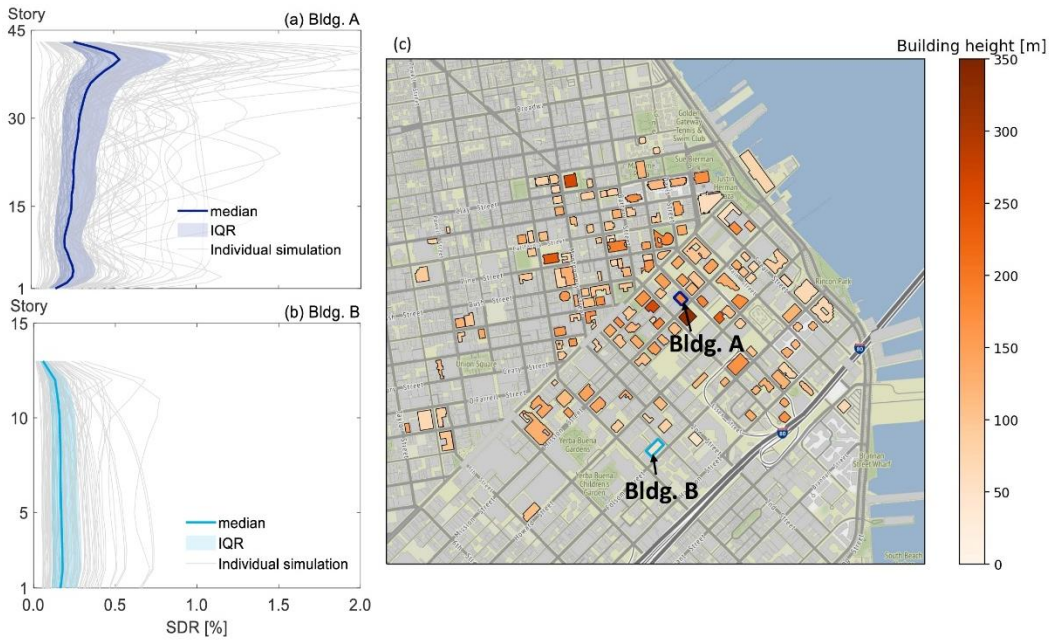

Figure 8: Effect of number of stories on simulated SDR results: maximum SDR profiles along the height of (a) Building A (43 stories) and (b) Building B (13 stories); (c) map of building heights.

The effect of changes in building location is illustrated in Figure 9c, which shows the maximum (along the building height) of the median (between all simulations) SDR for all buildings that were studied. Figure 9 also gives SDR profiles, shown in Figures 9a and 9b, calculated in the same manner as was done for Figures 8a and 8b, corresponding to two nearby buildings with similar building heights and very similar depths to bedrock but with very different building orientations. Building A has 41 stories and a height of 171 m and is located just north of Market Street, whereas Building B has 43 stories and a height of 168 m and is located just south of Market Street only about 150 m from Building A. As shown in Figure 9c, practically all buildings south of Market Street have their principal directions orientated parallel or perpendicular to Market Street, whereas those north of Market Street have their principal orientations relatively close to the North-South and East-West directions. For the HayWired earthquake scenario, whose epicenter is located approximately in the city of Oakland in the East Bay, the transverse orientation for these two buildings is approximately North-South and, therefore, not directly coincident with one of the principal directions of these two buildings. This leads to relatively similar demands for both buildings. For this particular earthquake scenario, the depth to bedrock and building height affect maximum median SDRs more than the different principal orientations of the buildings north and south of Market Street. Figures 9c, 8c, and 7b show that the southeastern buildings have relatively low depths to bedrock and smaller maximum median SDRs, while most of the buildings hovering around Market Street have larger depths to bedrock and larger maximum median SDRs. Taller buildings around Market Street underlain by sites with large depths to bedrock typically have 2nd modal building periods near the predominant period of the soil deposit, thereby significantly increasing SDRs in the upper portion of the buildings. On the other hand, sites with lower depths to bedrock have shorter site periods, which in general produce much smaller response spectral ordinates for the first few modes of the tall buildings considered in this study, and consequently result in smaller SDR demands.

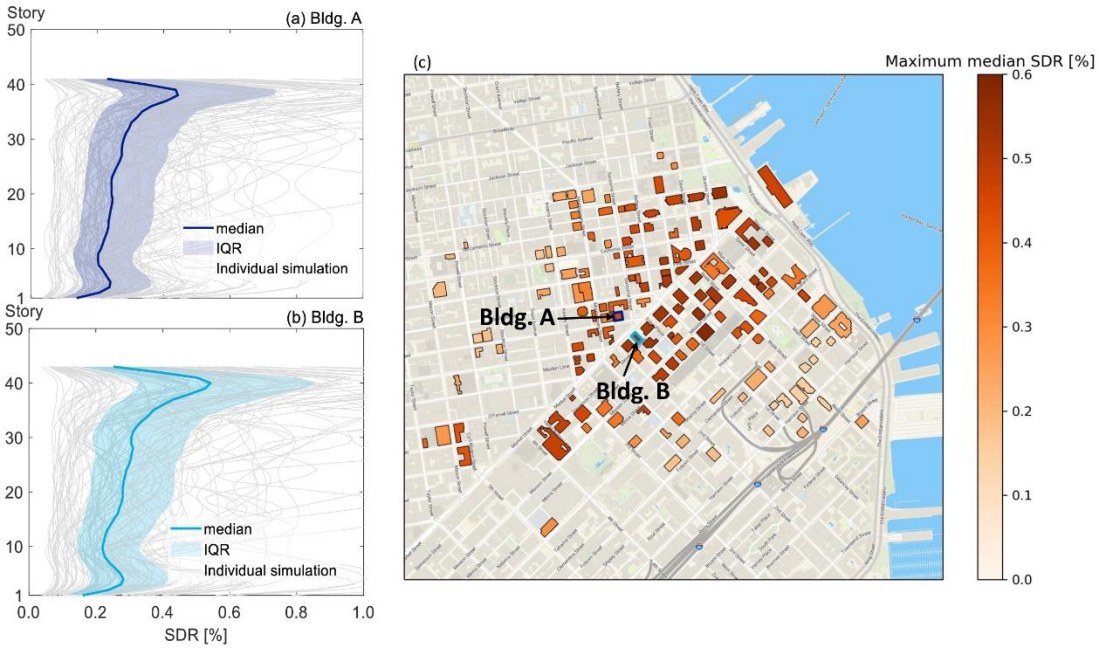

Figure 9: Effect of building location on simulated SDR demands: maximum simulated SDR profiles along the height of (a) Building A (41 stories) and (b) Building B (43 stories); (c) map of maximum median SDRs.

To highlight the effect that ground motion directionality may have on building response and possible damage, Figure 10 shows the results of a single building that is rotated to have two different orientations. For this example, the orientation of maximum spectral ordinates, that is, the orientation of RotD100, was set to be fixed in the North-South orientation, and 1,000 simulations were obtained for each principal orientation of the two hypothetical buildings. The orientation of the first building corresponds to the one present in most buildings located north of Market Street. For this first hypothetical building, shown in Figure 10a, the principal direction P_1 has an orientation that is only 10° from the orientation of RotD100, whereas the other principal direction P_2 has an orientation that is 80° away from the orientation of RotD100 and therefore, seismic demands in the P_1 orientation are expected to be significantly larger to those in P_2. This is particularly significant for tall buildings since ground motion polarization and ground motion directionality, in general, increase with increasing periods of vibration.[21] Figure 10a presents the resulting SDRs along the height in each principal orientation of the first hypothetical building, showing that indeed there are significantly larger (roughly 57% higher) mean and interquartile SDR demands for the P_1 principal direction, closer to the RotD100 orientation, than those computed for the P_2 principal direction. The figure also presents the probabilities of minor cracking of cold-formed steel framed gypsum partition walls[52] and probabilities of yielding of welded steel moment-resisting beam-to-column connections[51] as a function of height and principal orientation. Again, there are significant differences between both principal orientations, with the probabilities of damage of partition walls and beam-to-column connections in the orientation that is closer to North-South being, on average, 50% and 302% higher, respectively. The orientation of the second hypothetical building, shown in Figure 10b, corresponds to that present in most buildings located south of Market Street, where both building principal directions are at angular distances of approximately 45° to the RotD100 orientation. Unlike the first hypothetical building, in this case, the mean SDRs, probability of cracking of gypsum partition walls, and probability of yielding of beam-to-column connections are very similar in both principal directions, with the values in one of the orientations being only approximately on average 8%, 7%, and 40% higher than those in the other orientation, respectively.

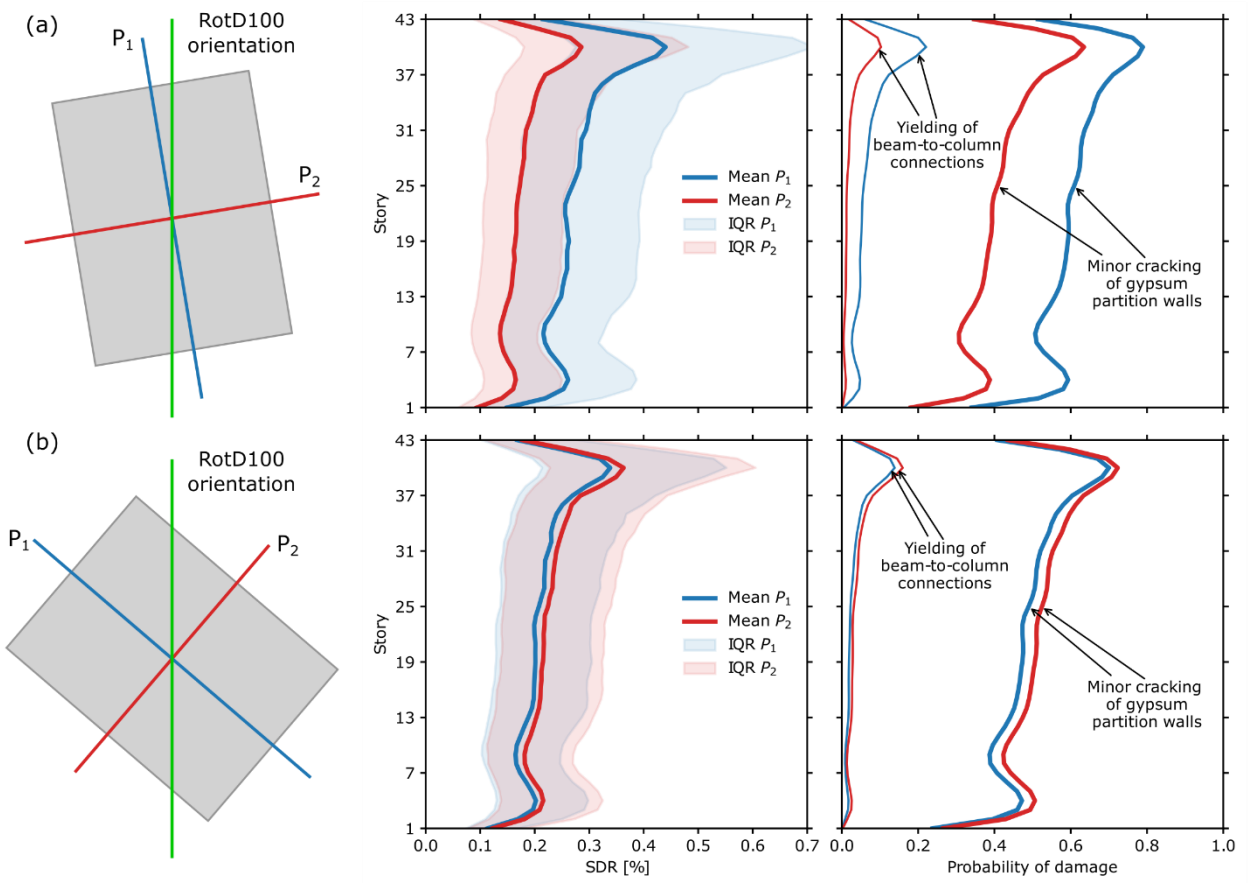

Figure 10: Distributions of SDR demands over the height of a building, probability of yielding of beam-to-column connections, and probability of minor cracking of gypsum partition walls in two identical buildings located at the same site but having different hypothetical orientations. The distributions were computed for the building oriented as buildings a) north of Market Street and b) south of Market Street while assuming the orientation of RotD100 to be North-South.

To study structural responses at a regional scale (i.e., for the complete building set), a single metric of SDR demand denoted as SDR_{max} is used to characterize the response of each building within a single simulation and it corresponds to the maximum SDR of the building, considering all stories and both principal orientations. Figure 11a shows the histogram of mean SDR_{max} over all 180 buildings for the 1,000 simulations. The mean SDR_{max} over all buildings from most simulations ranges between 0.15% and 1%, with its mean being 0.49%. To illustrate some of the results that can be obtained with the proposed regional seismic risk assessment framework, Figure 11b shows the probability that six different levels of SDR are surpassed in at least a given number of buildings.

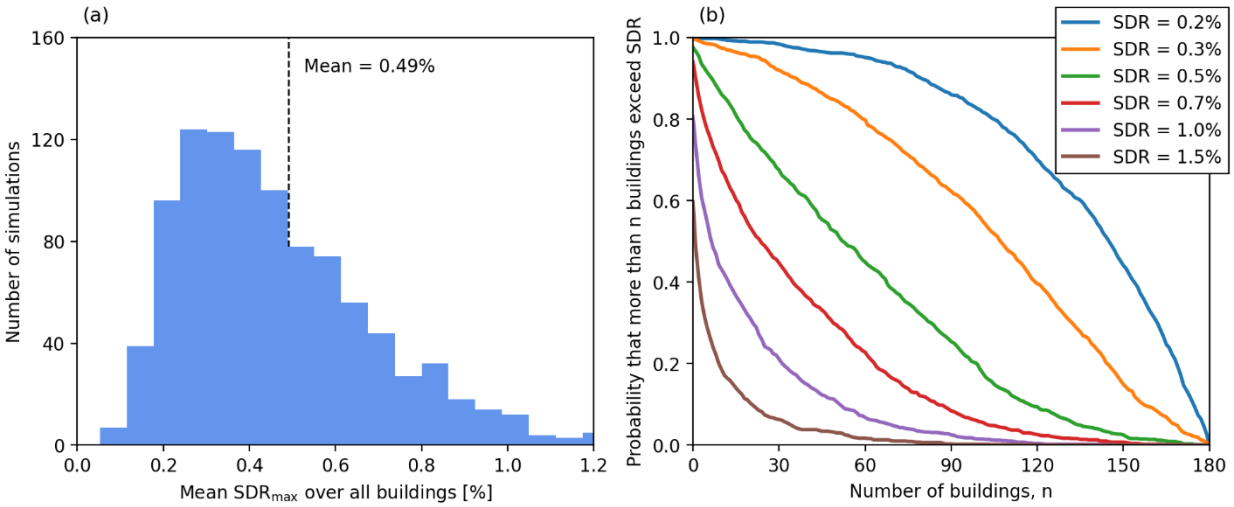

Figure 11: Maximum building story drift ratio in each building (SDR$_{max}$) from 1,000 simulations: (a) histogram of mean SDR$_{max}$ demands; (b) probability that at least a given number of buildings exceed a given level of SDR.

Similar regional-scale results were obtained for the probability of yielding of pre-Northridge beam-to-column connections and probability of minor cracking of gypsum partition walls, with the maximum probability of damage from all stories and from both principal orientations defined as Py$_{max}$ and Pc$_{max}$, respectively. Please note that these probabilities of damage are not the same as the probability that at least one component in the building suffers damage because this would require knowing the distribution of components in the buildings. The probabilities presented here are just the maximum probabilities of damage between all possible locations within the building (i.e., all stories and both principal orientations). Figure 12 shows the results for the maximum probabilities of yielding of beam-to-column connections, with Figure 12a being analogous to Figure 11b and Figure 12b showing different percentile lines for the fraction of buildings that surpass given levels of Py$_{max}$. The results show that, for example, the probability that 39 buildings have a Py$_{max}$ greater than 0.1 is 0.5, or equivalently, that the fraction of buildings that have a Py$_{max}$ greater than 0.1 has a median value of 0.22 (because there are 180 buildings). Similar results are shown in Figure 13 for the maximum probability of minor cracking of gypsum partition walls. As expected, the number of buildings that have significant damage probabilities is much higher for the gypsum partition walls than for yielding of beam-to-column connections because of the underlying fragility curves.

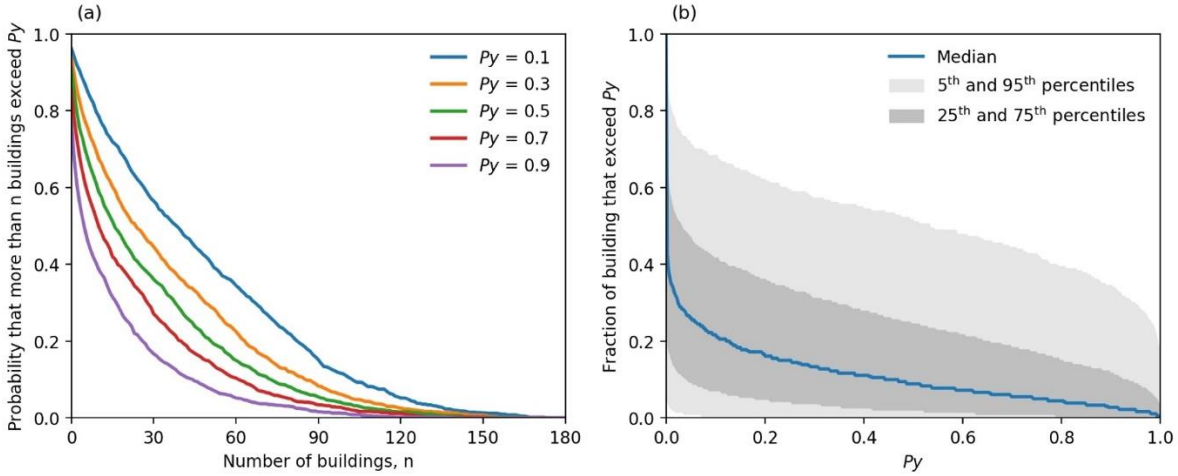

Figure 12: Maximum probability of yielding of pre-Northridge beam-to-column connections (Py) computed from 1,000 simulations: (a) probability that at least a given number of buildings exceed a given level of Py; (b) fraction of buildings that exceed given levels of Py.

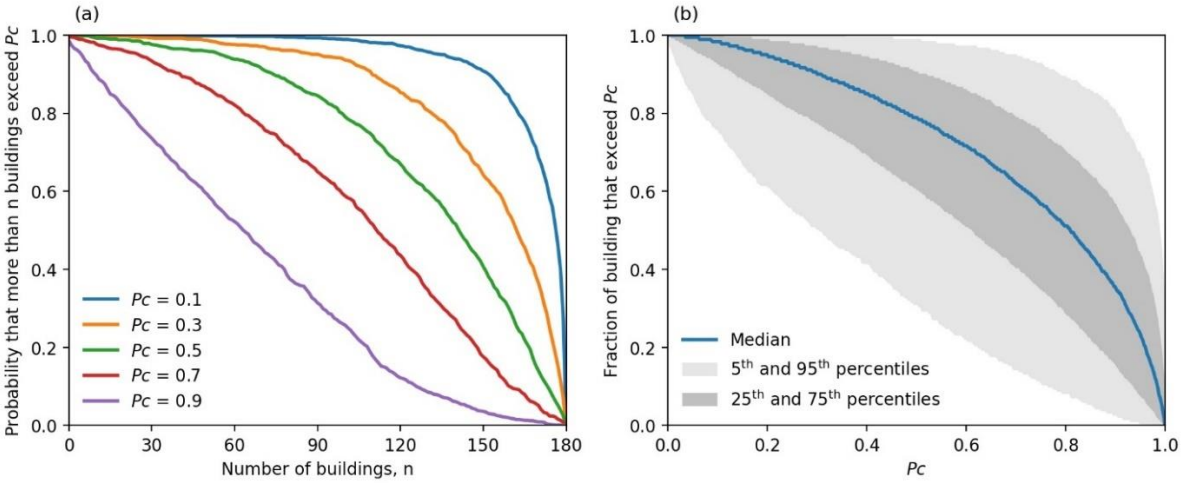

Figure 13: Maximum probability of cracking of gypsum partition walls (Pc) from 1,000 simulations: (a) probability that at least a given number of buildings exceed a given level of Pc; (b) fraction of buildings that exceed given levels of Pc.

4. Summary and Conclusions

This manuscript has presented a novel methodology based on the recently proposed Regional Performance-Based Earthquake Engineering (RPBEE) framework to assess the seismic risk of tall buildings at a regional scale. One of the main novelties in the proposed method lies in the use of simplified reduced-order models to estimate site response at hundreds or thousands of sites and to estimate the structural response of hundreds or thousands of buildings. The proposed approach is significantly more accurate than the use of modification factors to account for site effects or the use of vulnerability curves at the building level, yet it does not require a large amount of data nor computational cost to run a detailed site or structural analysis of each site and building. A simplified site response analysis procedure is implemented to improve ground motion intensity estimations from that of conventional ground motion models and physics-based ground motion simulations, which is especially important for soft-soil sites. For the site response analysis, a one-dimensional non-uniform shear beam model is used to obtain transfer functions of simplified soil profiles underneath each building. These shear beam models are defined by a very small number of parameters. For estimating building responses, the proposed methodology uses a simplified one-dimensional continuous non-uniform coupled shear-flexural beam, orientated in the two principal components of each building. The dynamic properties of each building are obtained from either ambient or seismic recorded responses or are sampled from empirically derived probability distributions, which are, in turn, used to obtain profiles of building responses along the height of each building. Finally, from the estimated response profiles, probabilities of damage can be computed for structural and non-structural components through fragility functions readily available in the literature. The framework also includes several other novel aspects. It explicitly considers, we believe for the first time, ground motion directionality, which is enabled by incorporating recent directionality models developed by two of the authors. Previous regional seismic loss assessments have neglected this directionality, that is, results are independent of the orientation of buildings or the orientation of buildings relative to the epicenter. Rock outcrop response spectra are simulated to account for both spatial correlation and correlation across periods at all sites simultaneously using recently developed spatial and spectral correlation models. Moreover, the framework accounts for the uncertainties associated with each step and propagates them to the final regional risk metrics.

The reader should note that the proposed framework relies on simplified one-dimensional linear elastic models to obtain the dynamic properties and response of both the soil deposits and buildings for all sites. Using nonlinear site response analyses in combination with nonlinear structural response models on a regional level for thousands of sites and buildings has been lacking and is, in general, not feasible due to the large computational effort involved in these analyses but primarily due to the required detailed information. This detailed information on soil profiles and buildings is commonly unavailable at the regional level, that is, for a large number of sites and buildings. Despite using simplified linear elastic models, the proposed framework can still estimate the seismic hazard, building responses, and building damages very well with very few required parameters. The proposed framework provides adequate results for situations in which the response is elastic or for cases where the non-linear response does not differ significantly

from the peak linear response, such as where the equal displacement approximation can be used. In other cases, the proposed framework can successfully identify sites or buildings where nonlinear models should be used.

To illustrate the use of the proposed framework, it was applied to a group of 180 tall buildings located in the Financial District of the city of San Francisco in California. These buildings were subjected to the seismic hazard produced by a hypothetical magnitude 7.0 scenario earthquake occurring on the Hayward Fault, approximately 15 km from the Financial District. This scenario was used to demonstrate the type of results that can be produced by the proposed framework, including building responses and damages along the height of individual buildings or maximum values on each building. These results highlight the effects of site conditions in which similar buildings located relatively close to each other can be subjected to important differences in hazard, response, and damage as a result of the depth to bedrock or building orientation. The case study also illustrates how large seismic demands and damage probabilities are often the result of specific combinations of building height and depth to bedrock. Although not explicitly shown in this manuscript, the output-building structural responses can also be used to estimate more informative seismic loss variables, such as economic losses, casualties, and downtimes.

Dedication

This paper is dedicated to the memory of Professors Helmut Krawinkler and Allin Cornell, former professors at Stanford University and now deceased, who made key contributions to the development of performance-based seismic assessment of individual structures and who were very interested in extending it to the regional level but, unfortunately, were not able to do so. Our study builds upon their utmost contributions and would not have been possible without them.

Acknowledgments

Financial aid to the first author to pursue doctoral studies at Stanford University under the supervision of the fourth author was provided by The Shah Family Fund in the School of Engineering from the Department of Civil and Environmental Engineering at Stanford University and The National Defense Science and Engineering Graduate Fellowship from the Department of Defense. The second author acknowledges the financial support of ANID FONDECYT Iniciación en Investigación Grant No. 11230463 and the UPS Endowment Fund for Transportation, Logistics, and Urban Issues at Stanford. Financial support to the third author was provided by the National Agency for Research and Development (ANID) / Doctorado Becas Chile under grant 2019-72200307 and the Nancy Grant Chamberlain Fellowship from the Department of Civil and Environmental Engineering at Stanford University. The financial aid provided is appreciated by all of the authors.

References

1. Freeman, J.R., 1932. *Earthquake damage and earthquake insurance.* First edition, McGraw-Hill Book Company, New York City.
2. Steinbrugge, K.V., 1982. Earthquakes, volcanoes and tsunamis: an anatomy of hazards. In *Earthquakes, volcanoes and tsunamis: An anatomy of hazards* (pp. 392-392). Skandia America Group, 1st edition, New York.
3. Reitherman, R., 1985. A review of earthquake damage estimation methods. *Earthquake Spectra*, *1*(4), pp.805-847.
4. Kircher, C.A., Reitherman, R.K., Whitman, R.V. and Arnold, C., 1997. Estimation of earthquake losses to buildings. *Earthquake Spectra*, *13*(4), pp.703-720.
5. Aslani, H. and Miranda, E. 2005. Probabilistic earthquake loss estimation and loss disaggregation in buildings. *Report No. 157*, John A Blume Earthquake Engineering Center, Stanford University, Stanford, California.
6. Kircher, C.A., Whitman, R.V. and Holmes, W.T., 2006. HAZUS earthquake loss estimation methods. *Natural Hazards Review*, *7*(2), pp.45-59.
7. Calvi, G.M., Pinho, R., Magenes, G., Bommer, J.J., Restrepo-Vélez, L.F. and Crowley, H., 2006. Development of seismic vulnerability assessment methodologies over the past 30 years. *ISET journal of Earthquake Technology*, *43*(3), pp.75-104.

8. Scawthorn, C., 2008. A brief history of seismic risk assessment. *Risk assessment, modeling and decision support: Strategic directions*, pp.5-81.
9. Kassem, M.M., Nazri, F.M. and Farsangi, E.N., 2020. The seismic vulnerability assessment methodologies: A state-of-the-art review. *Ain Shams Engineering Journal*, *11*(4), pp.849-864.
10. Hosseinpour, V., Saeidi, A., Nollet, M.J. and Nastev, M., 2021. Seismic loss estimation software: A comprehensive review of risk assessment steps, software development and limitations. *Engineering Structures*, *232*, p.111866.
11. Du, A., Wang, X., Xie, Y. and Dong, Y., 2023. Regional Seismic Risk and Resilience Assessment: Methodological Development, Applicability, and Future Research Needs–An Earthquake Engineering Perspective. *Reliability Engineering & System Safety*, p.109104.
12. Cornell C.A. and Krawinkler, H. 2000. Progress and challenges in seismic performance assessment. *PEER newsletter* No. 3(2), Pacific Earthquake Engineering Research (PEER) Center, Berkeley, California, pp. 1-4.
13. Krawinkler, H., 2002, A general approach to seismic performance assessment. In *Proceedings of International Conference on Advances and New Challenges in Earthquake Engineering Research* (Vol. 3, pp. 173-80). ICANCEER 2002, Hong Kong, August 19-20.
14. Krawinkler, H. and Miranda, E., 2004. Performance-based earthquake engineering. *Earthquake engineering: from engineering seismology to performance-based engineering*, *9*, CRC-press, pp.1-9.
15. ATC-13 (1985), "Earthquake damage evaluation data for California". Redwood City, CA: Applied Technology Council.
16. Federal Emergency Management Agency, 2012. Multi-hazard loss estimation methodology, earthquake model, Hazus-MH 2.1 technical manual. Technical report, Federal Emergency Management Agency, Mitigation Division, Washington, DC.
17. Heresi, P. and Miranda, E., 2022. Evaluation of relative seismic performance between one-and two-story houses. *Journal of Earthquake Engineering*, *26*(2), pp.857-886.
18. Heresi, P. and Miranda, E., 2023. RPBEE: Performance-based earthquake engineering on a regional scale. *Earthquake Spectra*, 39(3), pp.1328-1351.
19. Heresi, P. and Miranda, E., 2023. Regional-risk-targeted seismic design: A novel approach for earthquake resistant design. *Earthquake Engineering & Structural Dynamics*, *52*(13), pp.3983-4008.
20. Boore, D.M., 2010. Orientation-independent, nongeometric-mean measures of seismic intensity from two horizontal components of motion. *Bulletin of the Seismological Society of America*, *100*(4), pp.1830-1835.
21. Poulos, A. and Miranda, E., 2022. Probabilistic characterization of the directionality of horizontal earthquake response spectra. *Earthquake Engineering & Structural Dynamics*, *51*(9), pp.2077-2090.
22. Poulos, A. and Miranda, E., 2022. Proposal of orientation-independent measure of intensity for earthquake-resistant design. *Earthquake Spectra*, *38*(1), pp.235-253.
23. Sokolov, V. and Wenzel, F., 2013. Spatial correlation of ground motions in estimating seismic hazards to civil infrastructure. In *Handbook of seismic risk analysis and management of civil infrastructure systems* (pp. 57-78). Woodhead Publishing. Cambridge, Massachusetts.
24. Park, J., Bazzurro, P. and Baker, J.W., 2007. Modeling spatial correlation of ground motion intensity measures for regional seismic hazard and portfolio loss estimation. *Tenth International Conference on Application of Statistic and probability in civil engineering*, *2*, pp.1-8. ICASP10, Tokyo, July 31 – August 3.
25. Heresi, P. and Miranda, E., 2019. Uncertainty in intraevent spatial correlation of elastic pseudo-acceleration spectral ordinates. *Bulletin of Earthquake Engineering*, *17*, pp.1099-1115.
26. Boore, D.M., Stewart, J.P., Seyhan, E. and Atkinson, G.M., 2014. NGA-West2 equations for predicting PGA, PGV, and 5% damped PSA for shallow crustal earthquakes. *Earthquake Spectra*, *30*(3), pp.1057-1085.
27. Goda, K. and Hong, H.P., 2008. Spatial correlation of peak ground motions and response spectra. *Bulletin of the Seismological Society of America*, *98*(1), pp.354-365.
28. Baker, J.W. and Jayaram, N., 2008. Correlation of spectral acceleration values from NGA ground motion models. *Earthquake Spectra*, *24*(1), pp.299-317.
29. Goda, K. and Atkinson, G.M., 2010. Intraevent spatial correlation of ground-motion parameters using SK-net data. *Bulletin of the Seismological Society of America*, *100*(6), pp.3055-3067.
30. Aldea, S., Heresi, P. and Pastén, C., 2022. Within-event spatial correlation of peak ground acceleration and spectral pseudo-acceleration ordinates in the Chilean subduction zone. *Earthquake Engineering & Structural Dynamics*, *51*(11), pp.2575-2590.
31. Bodenmann, L., Baker, J.W. and Stojadinović, B., 2024. Accounting for ground motion uncertainty in empirical seismic fragility modeling. *Earthquake Spectra*, *40*(4). pp.2456-2474.

32. Gasparini, D.A. and Vanmarcke, E.H., 1976. Simulated earthquake motions compatible with prescribed response spectra. *MIT Department of Civil Engineering Research Report*, R76-4, Order No. 527, Cambridge, Massachusetts.
33. Rathje, E.M., Kottke, A.R. and Ozbey, M.C., 2005. Using inverse random vibration theory to develop input Fourier amplitude spectra for use in site response. In *16th International Conference on Soil Mechanics and Geotechnical Engineering: TC4 Earthquake Geotechnical Engineering Satellite Conference* (pp. 160-166). Osaka, September 12-16.
34. Alonso-Rodríguez, A. and Miranda, E., 2018. Assessment of effects of reductions of lateral stiffness along height on buildings modeled as elastic cantilever shear beams. *Journal of Earthquake Engineering*, *22*(4), pp.553-568.
35. Alonso-Rodríguez, A. and Miranda, E., 2016. Dynamic behavior of buildings with non-uniform stiffness along their height assessed through coupled flexural and shear beams. *Bulletin of Earthquake Engineering*, *14*(12), pp.3463-3483.
36. Garcia-Suarez, J. and Asimaki, D., 2020. On the fundamental resonant mode of inhomogeneous soil deposits. *Soil Dynamics and Earthquake Engineering*, *135*, p.106190.
37. Dakoulas, P. and Gazetas, G., 1985. A class of inhomogeneous shear models for seismic response of dams and embankments. *International Journal of Soil Dynamics and Earthquake Engineering*, *4*(4), pp.166-182.
38. Bantis, J.C. and Miranda, E., 2023. Evaluation of random-vibration procedures to estimate response spectral ordinates on soft soil sites from Fourier amplitude spectra. *Soil Dynamics and Earthquake Engineering*, *166*, p.107776.
39. Shahi, S.K. and Baker, J.W., 2014. NGA-West2 models for ground motion directionality. *Earthquake Spectra*, *30*(3), pp.1285-1300.
40. Poulos, A. and Miranda, E., 2023. Effect of style of faulting on the orientation of maximum horizontal earthquake response spectra. *Bulletin of the Seismological Society of America*, *113*(5), pp.2092-2105.
41. Poulos, A. and Miranda, E., 2023. Modification of ground-motion models to estimate orientation-dependent horizontal response spectra in strike-slip earthquakes. *Bulletin of the Seismological Society of America*, *113*(6), pp.2718-2729.
42. Cruz, C., 2017. *Evaluation of damping ratios inferred from the seismic response of buildings*, PhD thesis, Dept. of Civil and Environmental Engineering, Stanford University, Stanford, California.
43. Cruz, C. and Miranda, E., 2017. Evaluation of the Rayleigh damping model for buildings. *Engineering Structures*, *138*, pp.324-336.
44. Rezaeian, S., Bozorgnia, Y., Idriss, I.M., Abrahamson, N., Campbell, K. and Silva, W., 2014. Damping scaling factors for elastic response spectra for shallow crustal earthquakes in active tectonic regions: "Average" horizontal component. *Earthquake Spectra*, *30*(2), pp.939-963.
45. Rezaeian, S., Al Atik, L., Kuehn, N.M., Abrahamson, N., Bozorgnia, Y., Mazzoni, S., Withers, K. and Campbell, K., 2021. Spectral damping scaling factors for horizontal components of ground motions from subduction earthquakes using NGA-Subduction data. *Earthquake Spectra*, *37*(4), pp.2453-2492.
46. Dávalos, H., Miranda, E., Bantis, J. and Cruz, C., 2022. Response spectral damping modification factors for structures built on soft soils. *Soil Dynamics and Earthquake Engineering*, *154*, p.107153.
47. Bantis, J. and Miranda, E., 2024. Effect of Damping on Response Spectral Ordinates of Ground Motions Recorded on Soft Soils in the San Francisco Bay Area. *Soil Dynamics and Earthquake Engineering*. Submitted April 2024. Available at SSRN: https://ssrn.com/abstract=4807877.
48. Miranda, E. and Akkar, S.D., 2006. Generalized interstory drift spectrum. *Journal of structural engineering*, *132*(6), pp.840-852.
49. Kiureghian, A.D. and Nakamura, Y., 1993. CQC modal combination rule for high-frequency modes. *Earthquake Engineering & Structural Dynamics*, *22*(11), pp.943-956.
50. Taghavi-Ardakan, S. and Miranda, E. 2006. Probabilistic seismic assessment of floor acceleration demands in multi-story buildings. *Report No. 162*, John A Blume Earthquake Engineering Center, Stanford University, Stanford, California.
51. Ramirez, C.M., Lignos, D.G., Miranda, E. and Kolios, D., 2012. Fragility functions for pre-Northridge welded steel moment-resisting beam-to-column connections. *Engineering Structures*, *45*, pp.574-584.
52. Miranda, E., and Mosqueda, G., 2011. *Seismic fragility of building interior cold-formed steel framed gypsum partition walls*. Background Document FEMA P-58/BD-3.9.2. Applied Technology Council, Redwood City, California.
53. Federal Emergency Management Agency, 2012. Seismic performance assessment of buildings, methodology vol 1. Technical report, Federal Emergency Management Agency, Washington, DC.

54. Heresi, P. and Miranda, E., 2022. Structure-to-structure damage correlation for scenario-based regional seismic risk assessment. *Structural Safety*, *95*, p.102155.
55. ATC-119 (2018), "San Francisco Tall Buildings Study". Redwood City, CA: Applied Technology Council.
56. Detweiler, S.T. and Wein, A.M., 2018. The HayWired earthquake scenario: Engineering implications. *Scientific investigations report No.* 2017-5013-I-Q., United States Geological Survey, Reston, Virginia.
57. Stewart, J.P. and Seyhan, E., 2013. *Semi-empirical nonlinear site amplification and its application in NEHRP site factors*. PEER Report No. 2013/13, Pacific Earthquake Engineering Research Center, University of California, Berkeley, CA.
58. Afshari, K. and Stewart, J.P., 2016. Physically parameterized prediction equations for significant duration in active crustal regions. *Earthquake Spectra*, *32*(4), pp.2057-2081.
59. Byerly, P., Hester, J. and Marshall, K., 1931. The natural periods of vibration of some tall buildings in San Francisco. *Bulletin of the Seismological Society of America*, *21*(4), pp.268-276.
60. Schlocker, J., Radbruch, D.H. and Bonilla, M.G., 1954. *Preliminary bedrock-surface map of the San Francisco City area, California* (No. 54-274). US Geological Survey.